PNAS RESEARCH ARTICLE | EARTH, ATMOSPHERIC, AND PLANETARY SCIENCES
ENVIRONMENTAL SCIENCES

Mesozoic atmospheric CO_2 concentrations reconstructed from dinosaur tooth enamel

Dingsu Feng[a,b,1], Thomas Tütken[c], Eva Maria Griebeler[d], Daniel Herwartz[b], and Andreas Pack[a]

Affiliations are included on p. 6.

Edited by John Valley, University of Wisconsin-Madison, Madison, WI; received March 3, 2025; accepted June 9, 2025

Air-breathing vertebrates incorporate a fraction of isotopically anomalous air O_2 in their body water. The ^{17}O isotope anomaly of air O_2 (expressed as $\Delta'^{17}O_{air}$) is related to atmospheric CO_2 concentrations (pCO_2) and gross primary production (GPP). Tooth enamel records the $\Delta'^{17}O$ of body water and can thus preserve such paleo-pCO_2 or paleo-GPP information over geological time periods. Here, we demonstrate the potential of respective reconstructions of atmospheric pCO_2 or GPP from the triple oxygen isotope composition of fossil dinosaur tooth enamel. The data from unaltered enamel samples, along with an assumed modern GPP_t/GPP_0 ratio of 1 for the Mesozoic, suggest a mean Late Jurassic pCO_2 = 1,200 ± 150 ppmv and Late Cretaceous pCO_2 = 750 ± 200 ppmv. These estimates are in good agreement with other pCO_2 proxy data for the same time intervals. When utilizing a pCO_2 inferred from other proxies, tooth enamel $\Delta'^{17}O_{PO4}$ may also serve as a proxy for GPP. Using published pCO_2 data, we reconstructed GPP_t/GPP_0 ratios with 1.20 ± 0.17 for the Late Jurassic and 2.24 ± 0.96 for the Late Cretaceous, which would imply a 20 to 120% higher GPP in the Mesozoic than today. Overall, triple oxygen isotope analysis of fossil teeth of terrestrial amniotes can provide insights into past atmospheric greenhouse gas content and global primary productivity.

dinosaur teeth | Mesozoic atmosphere | CO_2 concentrations | $\Delta'^{17}O$ | GPP

Atmospheric carbon dioxide plays an important role in global climate throughout Earth's history. Arrhenius (1896) (1) first discussed that variations in atmospheric CO_2 concentrations can be related to climate changes in geological history. A close correlation between atmospheric CO_2 partial pressure (pCO_2) and air temperature is well established for the past ≈1 Ma from the ice core record of the Quaternary (2–4). Pre-Quaternary atmospheric CO_2 levels are estimated from mass balance models (5, 6) or various geological and geochemical proxies, such as paleosols, phytoplankton, stomata density, boron and calcium isotopes in marine carbonates, liverworts, and nahcolite (7, 8). Each of these proxies is associated with its individual limitations; thus, combining pCO_2 proxies and models is a viable means for refined pCO_2 reconstructions (7, 8). A new proxy is the triple oxygen isotope composition of bioapatite from air-breathing vertebrates (9–12).

Pioneering studies suggested using triple oxygen isotopes in sulfates (13), carbonates (14), and tooth enamel (9, 10) as proxy for the $\Delta'^{17}O$ of air. The latter can be used to obtain information about past atmospheric pCO_2 if gross primary productivity (GPP) is known, or conversely, if pCO_2 is known, to infer GPP (14). The negative $\Delta'^{17}O$ of air O_2 counterbalances the positive $\Delta'^{17}O$ of the stratospheric CO_2 and ozone reservoirs (15). Therefore, $\Delta'^{17}O$ of air O_2 decreases with increasing pCO_2. The negative anomaly of air O_2, in turn, is diluted by the flux of isotopically normal photosynthetic O_2, and hence, $\Delta'^{17}O_{air}$ increases with increasing GPP. Therefore, $\Delta'^{17}O$ of air O_2 can be used as proxy for either pCO_2 or GPP.

Pack et al. (9) demonstrated that air-breathing vertebrates record a fraction of the ^{17}O anomaly of air oxygen in their skeletal bioapatite. This is because the inhaled, isotopically anomalous O_2 is utilized for aerobic metabolism of food, and the respective ^{17}O anomaly is thus first transferred to the body water (BW) and subsequently incorporated from there into the bioapatite. The diagenesis-resistant tooth enamel thus provides a time capsule of the in vivo incorporated ^{17}O anomaly in ancient air O_2. Using this approach, Gehler et al. (10) constrained paleo-pCO_2 levels during the Paleocene–Eocene Thermal Maximum; assuming different scenarios for the GPP_{PETM}. Feng et al. (11, 12) reported data on bioapatite of modern terrestrial and marine mammals as well as of sharks and calculated taxon-specific oxygen mass balance models across a large body mass range, providing a thorough empirical baseline for the pCO_2 reconstruction from bioapatite of air-breathing vertebrates.

Significance

Paleoclimate is closely linked to atmospheric pCO_2. Quantifying ancient CO_2 levels, however, is challenging. Air-breathing vertebrates respire air O_2 and incorporate its isotope signature via body water into their hard tissues. Fossil tooth enamel can thus serve as a robust time capsule for ancient air O_2 isotope compositions. Air O_2 has an ^{17}O-anomaly that increases with increasing atmospheric pCO_2 and decreases with increasing gross primary productivity (GPP). Therefore, paleo-pCO_2 or paleo-GPP, respectively, can be determined by oxygen isotope measurements of fossil tooth enamel. Here, we reconstruct Mesozoic paleo-pCO_2 levels from the triple oxygen isotope composition of dinosaur teeth and obtain paleo-pCO_2 levels 2.5 to 4 times higher than preindustrial values. In addition, changes in the ^{17}O-anomaly could also point to substantial fluctuations in GPP of the biosphere.

Author contributions: D.F., T.T., and A.P. designed research; D.F. and A.P. performed research; D.F. contributed new reagents/analytic tools; D.F. analyzed data; and D.F., T.T., E.M.G., D.H., and A.P. wrote the paper.

The authors declare no competing interest.

This article is a PNAS Direct Submission.

[1]To whom correspondence may be addressed. Email: dingsu.feng@geo.uni-goettingen.de.

This article contains supporting information online at https://www.pnas.org/lookup/suppl/doi:10.1073/pnas.2504324122/-/DCSupplemental.

Published August 4, 2025.

In this study, we further extend the approach to modern birds and a reptile (i.e., Sauropsida), compare data to those of modern mammals and apply the results to extinct dinosaurs. The dinosaur teeth analyzed herein come from five different fossil sites in the United States, Canada, Morocco, Germany, and Tanzania, representing the two geological periods, the Late Jurassic (latest Oxfordian to Tithonian) as well as the Late Cretaceous (middle Cenomanian to late Maastrichtian). The specimens include genera such as sauropods (*Camarasaurus*, *Giraffatitan*, *Kaatedocus*, and *Europasaurus*), theropods (*Tyrannosaurus*, *Albertosaurus, Carcharodontosaurus,* and *Torvosaurus*), and ornithischians (*Edmontosaurus*) (see Dataset S1 for further details). We present high precision phosphate triple oxygen isotope data of dinosaur teeth, both enamel and dentine, which we first screen for diagenetic alteration. We use only the pristine enamel samples to reconstruct pCO_2 during the Mesozoic greenhouse climate, specifically for the Late Jurassic (Kimmeridgian to Tithonian) and Late Cretaceous (Campanian to Maastrichtian).

Our approach has a range of inherent uncertainties mainly originating from: i) the unknown Jurassic and Cretaceous GPP; and ii) errors related to physiological and environmental parameters. We demonstrate how these challenges can be overcome and how triple oxygen isotope data may also serve as a tool to study vertebrate paleophysiology.

1. Results

A list with detailed information on the taxonomy, provenance, body mass, and geological age (for the dinosaur specimens) of all analyzed modern and fossil Sauropsida bone and tooth samples is provided in Dataset S1.

The triple oxygen isotope data ($\Delta'^{17}O_{PO4}$ vs. $\delta^{18}O_{PO4}$) for bone bioapatite of modern birds are listed in Dataset S2. The bird data are plotted in Fig. 1 and are fully overlapping with those of modern mammals from ref. 12. The data point for the alligator falls at the upper end of the field covered by modern mammals and birds (Fig. 1).

The triple oxygen isotope data and the $\delta^{13}C$ and $\delta^{18}O_{CO3}$ values of the structural carbonate in the bioapatite of the dinosaur teeth are listed in Dataset S3. The offset between phosphate and carbonate oxygen isotope composition ($\delta^{18}O_{CO3}$-$\delta^{18}O_{PO4}$) typical for modern bioapatite is taken as an indicator to assess diagenetic alteration of the oxygen isotope composition of the fossil dinosaur teeth (12).

Dinosaur dentine and enamel $\Delta'^{17}O_{PO4}$ values show a large scatter with unaltered enamel (see *Discussion* for details) plotting toward the lower range of the field of modern mammals and birds, but reaching down to values as low as -300 ppm (Fig. 2), which represent the lowest values reported for vertebrates so far.

2. Discussion

2.1. Comparison of $\Delta'^{17}O_{PO4}$ of Modern Birds and Terrestrial Mammals. As illustrated in Fig. 1, triple oxygen isotope ratios of modern bird bioapatite plot in the same range as those of modern terrestrial mammals (12). Birds of similar size and feeding ecology typically have higher basal metabolic rates than terrestrial mammals (17). However, a higher metabolic rate alone does not necessarily lead to systematically lower $\Delta'^{17}O_{PO4}$ in birds. Instead, the relation between $\Delta'^{17}O_{PO4}$ of bioapatite and $\Delta'^{17}O_{air}$ of inhaled air is affected by a number of factors, including body mass and water intake. This relationship has been modeled as a function of body mass (allometric scaling) using a mass balance model (9, 12). The observed similarity in $\Delta'^{17}O_{PO4}$ between birds and mammals is likely due to the higher specific water flux of birds compared to mammals (19, 20), which counterbalances the effect of higher basal metabolic rates of birds.

The physiology of the studied dinosaurs is a priori unknown. However, birds and crocodiles are the closest living relatives of dinosaurs forming their extant phylogenetic bracket (21, 22). Birds are warm-blooded descendants of nonavian dinosaurs that evolved from small theropod ancestors and are considered the only surviving lineage of dinosaurs, making them "living dinosaurs" in a phylogenetic sense. Therefore, birds (i.e., avian dinosaurs) may be suitable analogs here. The alligator falls at the upper end of the field covered by modern mammals and birds (Fig. 1). Our triple oxygen isotope data of recent birds demonstrate that their oxygen mass balance resembles that of mammals (Fig. 1). As a first approximation, we thus apply the $\Delta'^{17}O_{PO4}$ vs. body mass relationship

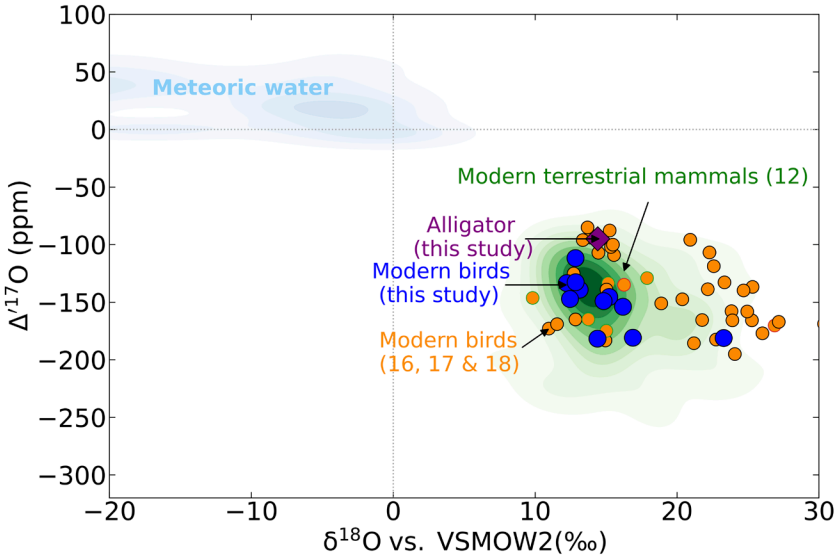

Fig. 1. Modern bird bone and alligator tooth enamel $\delta^{18}O_{PO4}$ vs. $\Delta'^{17}O_{PO4}$ data. Modern terrestrial mammals' enamel data (green shaded region) is from ref. 12 and represent the distribution of modern herbivores, omnivores, and carnivores from Central Europe (Germany), Africa, Australia, North America, and South America, with darker colors indicating a higher concentration of overlapping data. The 1σ SD of $\Delta'^{17}O_{PO4}$ values from modern mammal data (12) and the bird and reptile data from this study are ±34 ppm. Meteoric water (blue shaded region; for details and references, see Feng ref. 12) is displayed for comparison. The data displayed as orange circles are calculated bioapatite $\delta^{18}O_{PO4}$ and $\Delta'^{17}O_{PO4}$ values based on data from ref. 16 (carbonates in eggshells), ref. 17 (blood), and ref. 18 (carbonates in eggshells) (details about the calculation are provided in Datasets S4–S6, respectively).

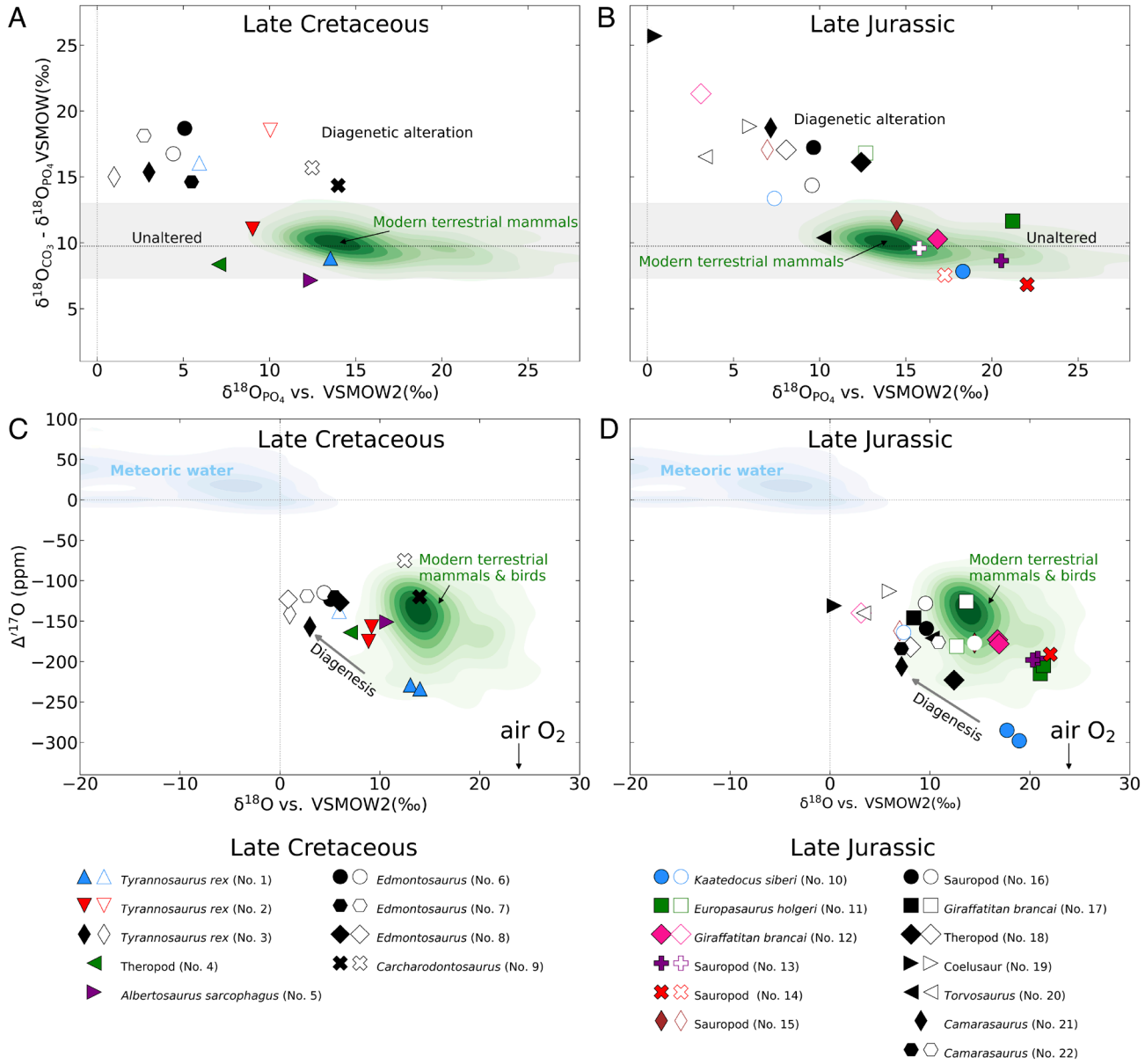

Fig. 2. Plots *A* and *B* illustrate the difference between the $\delta^{18}O$ values of the structural bioapatite carbonate ($\delta^{18}O_{CO3}$) and phosphate ($\delta^{18}O_{PO4}$) for dentine (open symbols) and enamel (filled symbols) of dinosaur tooth samples. The gray shaded areas represent the range from $7.4 \leq (\delta^{18}O_{CO3}\text{-}\delta^{18}O_{PO4}) \leq 13.0‰$ obtained from modern mammal bioapatite analyses (n = 96) (12). Filled black symbols indicate apparently diagenetically altered enamel. The majority of analyzed dentine samples (open symbols) show a clear sign of diagenetic alteration (i.e., $\delta^{18}O_{CO3}\text{-}\delta^{18}O_{PO4}$ offset > 13‰). Plots *C* and *D* illustrate the triple oxygen isotope composition ($\Delta'^{17}O_{PO4}$ vs. $\delta^{18}O_{PO4}$) of tooth enamel and dentine samples from this study. The green-shaded areas represent the combined data of modern birds (this study) and mammals from ref. 12. Note that diagenesis tends to shift $\Delta'^{17}O_{PO4}$ values toward more positive $\Delta'^{17}O$ values and more negative $\delta^{18}O$ values of meteoric water. Thus, $\Delta'^{17}O_{PO4}$-based pCO_2 reconstructions represent minimum estimates.

obtained from modern mammals (12). This allows reconstructing the $\Delta'^{17}O$ of air O_2 that was inhaled by the Late Jurassic and Late Cretaceous dinosaurs during their lifetime (see caption of Fig. 3 for details). The $\Delta'^{17}O$ of air can then be used to estimate either pCO_2 or GPP.

2.2. Preservation of Primary Oxygen Isotope Compositions in Fossil Teeth. The oxygen isotope composition of fossil bioapatite may undergo diagenetic alteration (23–27), which would obliterate the original isotope information. We have thus screened the studied fossil tooth samples for diagenetic alteration. In unaltered bioapatite, the difference between $\delta^{18}O_{CO3}$ of structural carbonate and $\delta^{18}O_{PO4}$ of the main phosphate component is 9.8 ± 1.5‰ (12, 23, 28–30). This difference can change during fossilization processes as the oxygen bound in the carbonate and phosphate group has different sensitivities against alteration processes, and hence, the $\delta^{18}O_{CO3}\text{-}\delta^{18}O_{PO4}$ offset is a good indicator for the diagenesis of the bioapatite oxygen isotope composition. As expected, most dentine samples show elevated $\delta^{18}O_{CO3}\text{-}\delta^{18}O_{PO4}$, reflecting their greater susceptibility to diagenesis compared to well-crystallized and more mineralized tooth enamel, for which many samples suggest that their oxygen isotope composition was not affected by alteration (Fig. 2 *A* and *B*).

Based on the $\delta^{18}O_{CO3}\text{-}\delta^{18}O_{PO4}$ criterion, we conclude that the tooth enamel samples of the Late Jurassic sauropods *Kaatedocus siberi*, *Europasaurus holgeri*, *Giraffatitan brancai* (No. 12), and three other sauropods indet. (Nos. 13, 14, and 15) as well as of the Late Cretaceous *Tyrannosaurus rex* (Nos. 1 and 2), theropod indet. (No. 4), and the *Albertosaurus sarcophagus* have not experienced a significant diagenetic alteration (Fig. 2) and thus can be

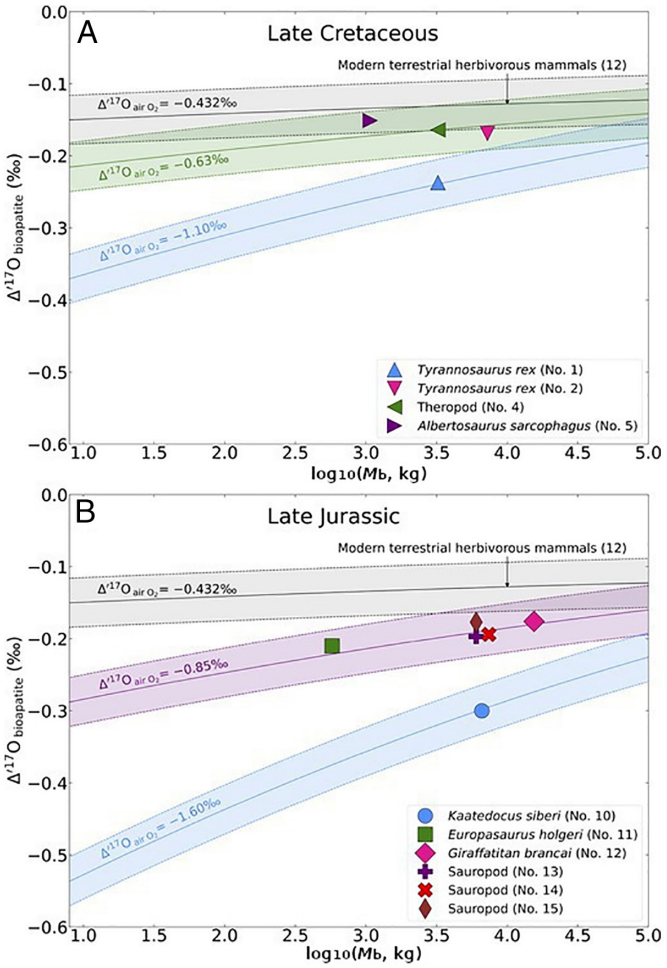

Fig. 3. The plot shows models of bioapatite $\Delta'^{17}O$ vs. logarithmic body mass (M_b, in kg) as calculated by ref. 12 for 42 recent taxa ("modern terrestrial herbivorous mammal line"), but solved for variable $\Delta'^{17}O_{air}$ to fit measured $\Delta'^{17}O_{PO4}$ values from well-preserved dinosaur enamel samples (see *SI Appendix*, Table S1 for details regarding the fossil samples). (*A*) Different theropods from the Late Cretaceous. The green curve represents the average $\Delta'^{17}O_{air}$ = –0.63‰ reconstructed from *Tyrannosaurus rex* (No. 2), theropod indet. (No. 4), and *Albertosaurus sarcophagus* (No. 5). The blue curve represents the $\Delta'^{17}O_{air}$ = –1.10‰ reconstructed from *T. rex* (No. 1). (*B*) Different sauropods from the Late Jurassic. The purple curve represents the average $\Delta'^{17}O_{air}$ = –0.85‰ reconstructed from *Europasaurus holgeri* (No. 11), *Giraffatitan brancai* (No. 12), and three other undetermined sauropod specimens (No. 13, 14, 15). The blue curve represents the extremely low $\Delta'^{17}O_{air}$ = –1.60‰ reconstructed from *Kaatedocus siberi* (No. 10). Dashed lines around modeled curves reflect a 1σ (SD) CI from the modern data from ref. 12 and the birds and reptile data from this study to ± 34 ppm in $\Delta'^{17}O_{PO4}$. The gray curve is the calibration line for modern terrestrial herbivorous mammals after ref. 12. Data are listed in Dataset S3.

used as a proxy archive for the $\Delta'^{17}O$ of air O_2 at the time when the dinosaur was alive. The dentine and altered enamel from dinosaurs exhibit higher $\Delta'^{17}O$ values than the unaltered enamel, as shown in Fig. 2 *C* and *D*, which suggests diagenesis tends to shift bioapatite $\Delta'^{17}O$ values toward more positive values. Hence, the $\Delta'^{17}O_{PO4}$ values of unaltered enamel represent an upper limit of the original in vivo compositions, and $\Delta'^{17}O_{PO4}$-based pCO_2 reconstructions should thus be regarded as a minimum estimate. In this contribution, we discarded all samples showing any sign of diagenesis from our discussion.

2.3. Triple Oxygen Isotope Ratios of Tooth Enamel as Paleo-$\Delta'^{17}O_{air}$ Proxy. Bone and tooth bioapatite (PO_4) precipitates from BW in oxygen isotope equilibrium (24). The isotope composition of BW is a function of in- (F_i) and outfluxes (F_j) and their respective isotope compositions ($\delta^{17,18}O_{i,j}$) (*SI Appendix*, section 2). For this study, the $\Delta'^{17}O$ of the ambient air O_2 is of particular interest. Oxygen fluxes can be modeled on the basis of allometric scaling laws (31) or physiological and environmental data for individual species (32). Isotopic compositions and fractionations are known from published datasets (9, 12).

Because animal physiology and environmental parameters show considerable variation even within populations of the same species in the same habitat (12), we follow a different approach rather than strictly applying allometric scaling of fluxes. Feng et al. (12) have modeled the composition of bioapatite for a set of 42 modern taxa of land-living herbivorous mammals comprising a broad range of body masses (M_b) ($0.002 \le M_b \le 6{,}000$ kg) as well as covering various environments and different physiologies. The 42 taxon-specific mass balance models were fitted to measured bioapatite $\delta^{18}O_{PO4}$ and $\Delta'^{17}O_{PO4}$ data of 42 modern herbivorous mammal taxa, living and breathing in today's atmosphere. Each mass balance was based on the model of Pack et al. (9). A value of modern $\Delta'^{17}O_{air}$ = –0.432 ± 0.015‰ (33) is applied in all these models, which are used to define the modern "herbivorous mammal curve" in a plot of $\Delta'^{17}O_{bioapatite}$ vs. body mass M_b (Fig. 3).

In certain periods of the Earth history, $\Delta'^{17}O_{air}$ may have been much lower than today (13). To simulate such scenarios of changing $\Delta'^{17}O_{air}$, we simultaneously lowered the $\Delta'^{17}O_{air}$ in all 42 mammal models and obtained characteristic $\Delta'^{17}O_{bioapatite}$ vs. M_b curves for different $\Delta'^{17}O_{air}$ (Fig. 3). Such simulations of the entire ensemble of these 42 BW models are used to infer ancient air $\Delta'^{17}O_{air}$ for a given $\Delta'^{17}O_{PO4}$. Specifically, for each well-preserved dinosaur enamel sample the measured $\Delta'^{17}O_{PO4}$ can be fitted onto such a curve by tuning $\Delta'^{17}O_{air}$ accordingly.

From the dataset of modern terrestrial mammals, birds, and the reptile, we deduce an overall uncertainty intrinsic to the $\Delta'^{17}O_{PO4}$ of 34 ppm. The uncertainty in reconstructed $\Delta'^{17}O_{air}$ is obtained by fitting the measured $\Delta'^{17}O_{PO4}$ to the upper and lower $\Delta'^{17}O_{air}$ error envelope of the respective $\Delta'^{17}O_{bioapatite}$ vs. M_b curve. The uncertainty in reconstructed $\Delta'^{17}O_{air}$ then is used to assess the respective uncertainties in paleo-CO_2 and/or GPP_t/GPP_0 (*SI Appendix*, Eq. **S4**). This practical approach to approximate an error for $\Delta'^{17}O_{air}$ is complemented by a comprehensive sensitivity analysis of the mass balance model provided in the Supplementary material.

2.4. $\Delta'^{17}O_{PO4}$ of Tooth Enamel: A Proxy for $\Delta'^{17}O_{air}$ and Thus Paleo-pCO_2 or Paleo-GPP. The enamel triple oxygen isotope data from Late Cretaceous theropod teeth of *T. rex* (No. 2), an unidentified theropod (No. 4), and *A. sarcophagus* suggest an overall common $\Delta'^{17}O_{air}$ = –0.63 ± 0.09‰, which is significantly lower than today (Fig. 3). Assuming a modern-day GPP_t/GPP_0 = 1, this transforms to a pCO_2 = 750 ± 200 ppmv (*SI Appendix*, Eq. **S4**). Varying the GPP_t/GPP_0 to 0.67 and 1.5 would yield Late Cretaceous pCO_2 of 500 ± 135 and 1,100 ± 300 ppmv (*SI Appendix*, Fig. S2), respectively. The data point of *T. rex* (No. 1) plots at a very low $\Delta'^{17}O_{PO4}$. Such a low $\Delta'^{17}O_{PO4}$ would imply a $\Delta'^{17}O_{air}$ as low as –1.10 ± 0.07‰, which would suggest a high pCO_2 = 1,800 ± 250 ppmv (at GPP_t/GPP_0 = 1).

The enamel triple oxygen isotope data from Late Jurassic sauropod teeth of *E. holgeri*, *G. brancai*, and the three undetermined sauropod specimens (No. 13, 14, 15) can be well-explained by a common $\Delta'^{17}O_{air}$ of –0.85 ± 0.07‰. Assuming a modern-day GPP_t/GPP_0 = 1, this transforms to a pCO_2 = 1,200 ± 150 ppmv (*SI Appendix*, Eq. **S4**). Setting the GPP_t/GPP_0 to 0.67 and 1.5 would yield Late Jurassic pCO_2 of 830 ± 100 and 1,800 ± 230 ppmv, respectively (*SI Appendix*, Fig. S2). The data for the diplodocid

K. siberi show significantly lower $\Delta'^{17}O_{PO4}$ than all the other dinosaurs from the Late Jurassic, which suggests $\Delta'^{17}O_{air}$ of –1.60 ± 0.11‰. This would correspond to a high pCO_2 = 2,900 ± 250 ppmv (at GPP_t/GPP_0 = 1).

Because diagenesis would unidirectionally tend to increase the $\Delta'^{17}O_{PO4}$, any diagenetic overprint would lead to an underestimation of the pCO_2 or GPP_t/GPP_0. Hence, low $\Delta'^{17}O_{PO4}$ values observed for the Late Jurassic *K. siberi* and Late Cretaceous *T. rex* (No. 1) are likely not the result of diagenetic alteration.

The reconstructed pCO_2 data for the Late Jurassic and Late Cretaceous agree well with other paleo-CO_2 proxy data for these periods. The apparently high pCO_2 values suggested by the low-$\Delta'^{17}O_{PO4}$ enamel samples from the Late Jurassic and Late Cretaceous are significantly higher than average values suggested by other proxies, but would still fall within the range of reconstructed values, in particular they fit to some high pCO_2 data inferred from soil carbonates (34, 35).

The $\Delta'^{17}O$ of air O_2 does not only reflect variations in pCO_2 but also variations in GPP_t/GPP_0 ratios. Using published pCO_2 estimates of Royer (7) and Beerling and Royer (8) of 1,500 ppmv for the Late Jurassic and 1,000 ppmv for the Late Cretaceous from other proxy data, respective GPP_t/GPP_0 estimates are 1.20 ± 0.17 ($\Delta'^{17}O_{air}$ = –0.85 ± 0.07‰, *SI Appendix*, Eq. **S4**) for the Late Jurassic and 2.24 ± 0.96 ($\Delta'^{17}O_{air}$ = –0.63 ± 0.09‰, *SI Appendix*, Eq. **S4**) for the Late Cretaceous.

2.5. Dinosaur Enamel Samples with Low $\Delta'^{17}O_{PO4}$. One explanation for the *T. rex* (No. 1) and *K. siberi* having lower $\Delta'^{17}O_{PO4}$ than other near-contemporaneous dinosaurs is fluctuations in $\Delta'^{17}O_{air}$ at geologically short time scales, i.e., $\Delta'^{17}O_{air}$ was low at the time during which these animals lived. For the Late Cretaceous (Maastrichtian), *T. rex* (No. 1) would then suggest a pCO_2 1,800 ± 300 ppmv, which is 1,000 ppmv higher than what is obtained from other theropod dinosaurs (including other *T. rex* specimens) of the same time period (Fig. 4). For the Late Jurassic *K. siberi*, the reconstructed pCO_2 is 1,700 ppmv higher than from specimens of other sauropod taxa of the same time period (Fig. 4).

The Earth's pCO_2 record is dynamic and comprises natural variations including spikes, for instance, during hyperthermals such as the Paleocene-Eocene thermal maximum. For this time interval, a sudden increase in pCO_2 by 1,130 ppmv (36) had been suggested. As shown in ref. 37, the $\Delta'^{17}O_{air}$ of air O_2 reacts to changes in pCO_2 within a few thousands of years. The Late Cretaceous and the Late Jurassic specimens may well have lived within a time span covering a short-term pulse in pCO_2 (e.g., the end-Cretaceous Deccan trap volcanism, 38–41) that could, in principle, be recorded in $\Delta'^{17}O_{PO4}$ of dinosaur tooth enamel. Alternatively, these individuals represent outliers in terms of paleoenvironment, physiology, and/or behavior. We hereafter explore this second scenario.

For the Late Cretaceous *T. rex* (No. 1), the comparably high $\delta^{18}O_{PO4}$ (Fig. 2*C*) hints toward dryer climates with evaporatively ^{18}O-enriched drinking water (14, 18). The sensitivity analysis demonstrates that drinking water composition and flux are dominant factors controlling the oxygen isotope composition, in particular for the large animals (*SI Appendix*, section 3.1.5). Surface water that is enriched in ^{18}O also drives $\delta^{18}O_{FW}$ of water in food and $\delta^{18}O_F$ oxygen in carbohydrates, fats, and proteins to higher $\delta^{18}O$ values. As the enrichment in ^{18}O is related to evaporation, these oxygen sources come along with a lower $\Delta'^{17}O$ (42). Additionally, the restricted availability of drinking water in such arid settings could also result in a lower flux of drinking water F_{DW} and hence a higher portion of metabolic water F_A with low $\Delta'^{17}O_A$. The respective effect on $\Delta'^{17}O_{BW}$ in BW is demonstrated by Hu et al. (18), who present data (Dataset S6) from the Australian emu reflecting a wide range of drinking water compositions. The animals with high $\delta^{18}O$ also comprise low $\Delta'^{17}O$ with the total emu dataset covering an 80 ppm range in $\Delta'^{17}O$. From these observations, we caution that the reconstructed low $\Delta'^{17}O_{air}$ from *T. rex* (No. 1) could at least partially reflect an artifact from a rather harsh paleoenvironment for *T. rex* (No. 1). Hence, this individual pCO_2 estimate may be inaccurate (i.e., represent an overestimation).

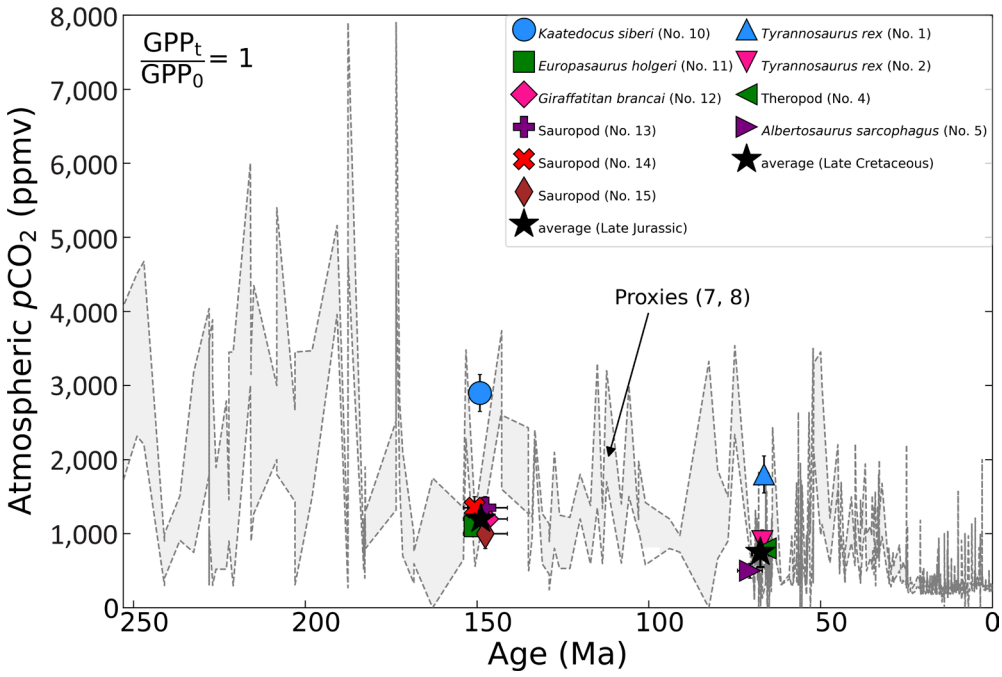

Fig. 4. Plot of pCO_2 (ppmv) vs. time in millions of years (Ma) from a compilation of different available pCO_2 proxies (7, 8). Colored symbols reflect the pCO_2 concentrations reconstructed from well-preserved dinosaur enamel samples. Black stars: average pCO_2 during the Late Jurassic and Late Cretaceous reconstructed from the dinosaur tooth enamel assuming a GPP_t/GPP_0 = 1.

In contrast to the Late Cretaceous *T. rex* (No. 1), the low $\Delta'^{17}O_{PO4}$ value for the Late Jurassic sauropod *K. siberi* (No. 10) is not associated with elevated $\delta^{18}O_{PO4}$, but plot within the $\delta^{18}O_{PO4}$ range measured for the other Late Jurassic sauropod tooth enamel samples (Fig. 3). In order to explore whether physiological effects can explain the low $\Delta'^{17}O_{PO4}$ of this specimen, we provide detailed BW modeling in the *SI Appendix*. We outline a range of approaches to approximate $\delta^{18}O_{DW}$ and drinking water amount as well as metabolic rates. We test these assumptions by comparing the results of the BW model to the actual data. The allometric scaling relations on metabolic rates vs. body mass of mammals and birds reveal rather similar estimates for *K. siberi* (No. 10) and the reptile scaling relationship calculates only a 50% lower rate (using data from ref. 43). Respective mass balance model fits can be achieved with drinking water flux of 70 L d^{-1} (reptile, 3,885 mol O/d) to 150 L d^{-1} (mammal, 8,324 mol O/d), corresponding to 1 to 3% of respective M_b (*SI Appendix*, Fig. S8). This modeling was accomplished using the $\Delta'^{17}O_{air}$ reconstruction used herein and suggested a $\Delta'^{17}O_{air} = -1.60 \pm 0.11$‰.

We have been unable to fit the mass balance model results to the analyzed tooth enamel data using the mean $\Delta'^{17}O_{air} = -0.85 \pm 0.07$‰ determined for the other Late Jurassic sauropods (*SI Appendix*, Fig. S9). Therefore, we conclude that *K. siberi* indeed records an unusually low $\Delta'^{17}O_{air} = -1.60 \pm 0.11$‰, possibly reflecting a spike in pCO_2 and/or a decline in GPP. More, well-stratified specimens from the Morrison Formation in North America need to be analyzed to further assess this hypothesis as other near-contemporaneous sauropods from the Tendaguru Formation in East Africa do not record such low $\Delta'^{17}O_{air}$.

3. Conclusions

The triple oxygen isotope data ($\Delta'^{17}O_{PO4}$, $\delta^{18}O_{PO4}$) of modern birds agree with data from a large variety of modern terrestrial mammals covering a large body mass range and a broad ecological spectrum (12). We conclude that the $\Delta'^{17}O_{PO4}$ vs. body mass relationship applies to air-breathing terrestrial amniotes in general and can thus also be used to reconstruct Mesozoic atmospheric $\Delta'^{17}O_{air}$ values from well-preserved dinosaur tooth enamel. For the Late Jurassic (152 to 143 Ma), sauropod tooth enamel data suggest $pCO_2 = 1{,}200 \pm 150$ ppmv (at $GPP_t/GPP_0 = 1$) or a $GPP_t/GPP_0 = 1.20 \pm 0.17$ (fixing pCO_2 at 1,500 ppmv based on other proxies). For the Late Cretaceous (73 to 66 Ma), our theropod tooth enamel data suggest an average $pCO_2 = 750 \pm 200$ ppmv (at $GPP_t/GPP_0 = 1$) or a $GPP_t/GPP_0 = 2.24 \pm 0.96$ (fixing pCO_2 at 1,000 ppmv based on other proxies). For both periods, one specimen exhibits considerably lower $\Delta'^{17}O_{PO4}$. In the case of the Late Cretaceous *T. rex* from the Lance Formation, this could be related to an evaporatively influenced drinking water source, as indicated by the high $\delta^{18}O_{PO4}$ of this specimen. In the second case of the Late Jurassic sauropod *K. siberi* from the Morrison Formation, the low $\Delta'^{17}O_{PO4}$ is likely related to a short-term fluctuation in $\Delta'^{17}O_{air}$ from −0.85 ± 0.07‰ to −1.60 ± 0.11‰, which may well be related to temporal high emission of CO_2 into the paleoatmosphere. Studies of larger sets of triple oxygen isotope data of fossil tooth enamel of land-living vertebrates can now be used to reconstruct the pCO_2 evolution of the atmosphere or (in concert with other pCO_2 proxy data) provide a tool to quantify changes in GPP. But this approach may also help to reveal differences in physiology and changing environmental parameters affecting these terrestrial vertebrates.

4. Materials and Methods

4.1. Definitions. VSMOW2 denotes the international reference material Vienna Standard Mean Ocean Water 2. Oxygen isotope anomalies are expressed with the $\Delta'^{17}O$ (Eq. **1**) notation. $\Delta'^{17}O$ is defined by the deviation of a sample with linearized forms of the δ-notations (44–46) from a given reference line (RL) with a particular slope (λRL) as follows:

$$\Delta'^{17}O_{0.528} = 1{,}000 \times \ln\left(\frac{\delta^{17}O^{sample}_{VSMOW2}}{1{,}000} + 1\right) - \lambda_{RL} \times 1{,}000 \times \ln\left(\frac{\delta^{18}O^{sample}_{VSMOW2}}{1{,}000} + 1\right). \quad [1]$$

A λ_{RL} of 0.528 is used in this study. All errors are reported as 1σ SD.

4.2 Materials and Methods. Oxygen isotopes of bones were analyzed from 10 different species of modern avian dinosaurs (i.e., birds) from Germany and Africa, as well as from 22 tooth enamel samples of fossil nonavian dinosaur taxa from the Late Cretaceous [*T. rex* (n = 3), theropod indet., *A. sarcophagus*, *Edmontosaurus* (n = 3), and *Carcharodontosaurus*], and from the Late Jurassic [*K. siberi*, *E. holgeri*, *G. brancai*, diplodocid sauropods (n = 5), theropods indet. (n = 2), *Torvosaurus*, *Camarasaurus* (n = 2)], as well as from one modern alligator for comparison. A detailed overview on the modern and fossil samples, including their taxonomy, body mass, provenance, stratigraphy, and geological age, is presented in the Dataset S1. We report 1σ errors throughout this study.

The bulk carbon ($\delta^{13}C$) and oxygen ($\delta^{18}O_{C03}$) isotope compositions of the structural carbonate group were analyzed by means of phosphoric acid digestion and CO_2 gas source mass spectrometry with $\delta^{18}O$ reported relative to VSMOW2 and $\delta^{13}C$ relative to VPDB (28). The triple oxygen isotope analyses of the bulk phosphate follow the laser fluorination protocol described in detail in ref. 11. All phosphate oxygen isotope data reported herein are reported relative to VSMOW2 and normalized to San Carlos Olivine with $\delta^{18}O = 5.3$‰ and $\Delta'^{17}O_{0.528} = -52$ ppm (47–49). The internal reference material AG-Lox (enamel of a molar from an African elephant, *Loxodonta africana*) was run several times in each analytical session, suggesting uncertainties of ±0.63‰ for $\delta^{18}O_{PO4}$ and ± 11 ppm for $\Delta'^{17}O_{PO4}$ (1SD, n = 162) (11, 12). All $\delta^{17}O_{PO4}$, $\delta^{18}O_{PO4}$, and $\Delta'^{17}O_{PO4}$ data are presented in Datasets S2 and S3, along with further details on the respective analytical procedures.

Data, Materials, and Software Availability. All study data are included in the article and/or supporting information.

ACKNOWLEDGMENTS. We thank Gerhard Hundertmark, Gisa Heinemann, and Dr. Gert Tröster for their support in the bird sample collection in the Zoologisches Museum of the University of Göttingen. We thank Hans-Jakob Siber (Sauriermuseum Aathal), Daniela Schwarz (Naturkundemuseum Berlin), Don Henderson (Tyrell Museum Drumheller), Anne Schulp (Naturalis Leiden), Nils Knötschke (Dinopark Münchehagen), and Alexander Gehler (Geowissenschaftliches Museum Göttingen) for kindly providing the dinosaur teeth for isotope analysis. Special thanks go to Martin Sander and Emanuel Tschopp for detailed information on sauropod taxonomy and body mass as well as providing valuable information on sauropod femur length and stratigraphic settings as well as helpful discussions. Dennis Kohl is thanked for his technical support, and Niklas Löffler is thanked for his constructive suggestions. This study was funded by the German Science Foundation (AP, PA909/20-1). D.H. was supported by his DFG Heisenberg grant (HE 6357/4-1). T.T. acknowledges funding through the VeWA consortium (Past Warm Periods as Natural Analogues of our high-CO_2 Climate Future) by the LOEWE program of the Hessen Ministry of Higher Education, Research and the Arts, Germany and from the European Research Council under the European Union's Horizon 2020 research and innovation program (grant agreement no. 681450).

Author affiliations: [a]Abteilung Geochemie & Isotopengeologie, Geowissenschaftliches Zentrum, Georg-August-Universität, Göttingen D-37077, Germany; [b]Institut für Geowissenschaften, Ruhr-Universität Bochum, Bochum D-44801, Germany; [c]Institut für Geowissenschaften, AG Angewandte und Analytische Paläontologie, Universität Mainz, Mainz D-55128, Germany; and [d]Institut für Organismische und Molekulare Evolutionsbiologie, Universität Mainz, Mainz D-55128, Germany

1. S. Arrhenius, On the influence of carbonic acid in the air upon the temperature on the ground. *Philos. Mag.* **41**, 237–279 (1896).
2. J. R. Petit *et al.*, Climate and atmospheric history of the past 420, 000 years from the Vostok ice core, Antarctica. *Nature* **54**, 349–392 (1999).
3. D. Lüthi *et al.*, High-resolution carbon dioxide concentration record 650, 000–800, 000 years before present. *Nature* **453**, 379–382 (2008).
4. G. L. Foster, D. L. Royer, D. J. Lunt, Future climate forcing potentially without precedent in the last 420 million years. *Nat. Commun.* **8**, 14845 (2017).
5. R. A. Berner, Inclusion of the weathering of volcanic rocks in the GEOCARBSULF model. *Am. J. Sci.* **306**, 295–302 (2006).
6. R. A. Berner, GEOCARBSULF: A combined model for Phanerozoic atmospheric O_2 and CO_2. *Geochim. Cosmochim. Acta* **39**, 569–584 (2006).
7. D. L. Royer, CO_2-forced climate thresholds during the Phanerozoic. *Geochim. Cosmochim. Acta* **39**, 569–584 (2006).
8. D. J. Beerling, D. L. Royer, Convergent cenozoic CO_2 history. *Nat. Geosci.* **4**, 418–420 (2011).
9. A. Pack, A. Gehler, A. Süssenberger, Exploring the usability of isotopically anomalous oxygen in bones and teeth as paleo-CO_2-barometer. *Geochim. Cosmochim. Acta* **102**, 306–317 (2013).
10. A. Gehler, P. D. Gingerich, A. Pack, Temperature and atmospheric CO_2 concentration estimates through the PETM using triple oxygen isotope analysis of mammalian bioapatite. *Proc. Natl. Acad. Sci. U.S.A.* **113**, 7739–7744 (2016).
11. D. Feng, T. Tütken, N. Löffler, G. Tröster, A. Pack, Isotopically anomalous metabolic oxygen in marine vertebrates as physiology and atmospheric proxy. *Geochim. Cosmochim. Acta* **328**, 85–102 (2022).
12. D. Feng *et al.*, Triple oxygen isotopes of modern terrestrial mammalian tooth enamel–New implications for paleoenvironmental and physiological research. *Geochim. Cosmochim. Acta* **365**, 21–34 (2024).
13. H. Bao, J. Lyons, C. Zhou, Triple oxygen isotope evidence for elevated CO_2 levels after a Neoproterozoic glaciation. *Nature* **54**, 349–392 (2008).
14. V. J. Hare *et al.*, Triple oxygen isotopes in eggshell carbonate as a proxy of late Cenozoic CO_2 and primary productivity. *Geochim. Cosmochim. Acta* **399**, 48–63 (2025).
15. B. Luz, E. Barkan, M. L. Bender, M. H. Thiemens, K. A. Boering, Triple-isotope composition of atmospheric oxygen as a tracer of biosphere productivity. *Nature* **54**, 349–392 (1999).
16. B. Passey *et al.*, Triple oxygen isotopes in biogenic and sedimentary carbonates. *Geochim. Cosmochim. Acta* **141**, 1–25 (2014).
17. P. Sabat *et al.*, Triple oxygen isotope measurements ($\Delta'^{17}O$) of body water reflect water intake, metabolism and $\delta^{18}O$ of ingested water in passerines. *Front. Physiol.* **12**, 710026 (2021).
18. H. Hu, B. Passey, S. B. Lehmann, N. E. Levin, B. J. Johnson, Modeling and interpreting triple oxygen isotope variations in vertebrates, with implications for paleoclimate and paleoecology. *Chem. Geol.* **642**, 1–20 (2023).
19. S. Daan, D. Masman, A. Groenewold, Avian basal metabolic rates: Their association with body composition and energy expenditure in nature. *Am. J. Physiol. Cell Physiol.* **259**, 333–340 (1990).
20. J. B. Williams, B. I. Tieleman, Flexibility in basal metabolic rate and evaporative water loss among hoopoe larks exposed to different environmental temperatures. *J. Exp. Biol.* **203**, 3153–3159 (2000).
21. B. K. McNab, Food habits and the basal rate of metabolism in birds. *Oecologia* **77**, 343–349 (1988).
22. Q. Ji, S. Ji, On the discovery of the earliest fossil bird in China (*Sinosauropteryx* gen. nov.) and the origin of birds. *Chin. Geol.* **233**, 30–33 (1996).
23. P. Iacumin, H. Bocherens, A. Mariotti, A. Longinelli, Oxygen isotope analyses of co-existing carbonate and phosphate in biogenic apatite: A way to monitor diagenetic alteration of bone phosphate? *Earth Planet. Sci. Lett.* **142**, 1–6 (1996).
24. Y. Kolodny, B. Luz, O. Navon, Oxygen isotope variations in phosphate of biogenic apatites, I. Fish bone apatite–rechecking the rules of the game. *Earth Planet. Sci. Lett.* **64**, 398–404 (1983).
25. A. Shemesh, Y. Kolodny, B. Luz, Oxygen isotope variations of biogenic apatites, II. Phosphorite rocks. *Earth Planet. Sci. Lett.* **64**, 405–416 (1983).
26. Z. D. Sharp, V. Atudorei, H. Furrer, The effect of diagenesis on oxygen isotope ratios of biogenic phosphates. *Am. J. Sci.* **300**, 222–237 (2000).
27. A. G. Kral, T. Geisler, M. Wiedenbeck, P. Guagliardo, T. Tütken, Phosphate uptake is an essential process for rapid bone mineralization during early diagenesis–evidence from bone alteration experiments. *Geochim. Cosmochim. Acta.* **375**, 173–185 (2024).
28. C. A. Chenery, V. Pashley, A. L. Lamb, H. J. Sloane, J. A. Evans, The oxygen isotope relationship between the phosphate and structural carbonate fractions of human bioapatite. *Rapid Commun. Mass Spectrom.* **26**, 309–319 (2012).
29. A. Gehler, T. Tütken, A. Pack, Oxygen and carbon isotope variations in a modern rodent community–Implications for paleoenvironmental reconstructions. *PLoS ONE* **7**, e49531 (2012).
30. R. A. Eagle *et al.*, Dinosaur body temperatures determined from isotopic (^{13}C–^{18}O) ordering in fossil biominerals. *Science* **333**, 443–445 (2011).
31. D. J. Bryant, P. N. Froelich, A model of oxygen isotope fractionation in body water of large mammals. *Geochim. Cosmochim. Acta* **59**, 4523–4537 (1995).
32. M. J. Kohn, Predicting animal $\delta^{18}O$: Accounting for diet and physiological adaptation. *Geochim. Cosmochim. Acta* **60**, 4811–4829 (1996).
33. A. Pack, Isotopic traces of atmospheric O_2 in rocks, minerals, and melts. *Rev. Mineral. Geochem.* **86**, 217–240 (2021).
34. D. D. Ekart, T. E. Cerling, I. P. Montanez, N. J. Tabor, A 400 million year carbon isotope record of pedogenic carbonate; implications for paleoatmospheric carbon dioxide. *Am. J. Sci.* **299**, 805–827 (1999).
35. L. Nordt, S. Atchley, S. Dworkin, Terrestrial evidence for two greenhouse events in the latest Cretaceous. *GSA Today* **4**, 9 (2003).
36. B. J. Fletcher, S. J. Brentnall, C. W. Anderson, R. A. Berner, D. J. Beerling, Atmospheric carbo dioxide linked with Mesozoic and early Cenozoic climate change. *Nat. Geosci.* **1**, 43–48 (2008).
37. E. D. Young, L. Y. Yeung, I. E. Kohl, On the $\Delta^{17}O$ budget of atmospheric O_2. *Geochim. Cosmochim. Acta* **135**, 102–125 (2014).
38. D. J. Beerling, B. H. Lomax, D. L. Royer, G. R. Upchurch Jr., L. R. Kump, An atmospheric pCO_2 reconstruction across the Cretaceous-Tertiary boundary from leaf megafossils. *Proc. Natl. Acad. Sci. U.S.A.* **99**, 7836–7840 (2002).
39. S. V. Petersen, A. Dutton, K. C. Lohmann, End-cretaceous extinction in Antarctica linked to both Deccan volcanism and meteorite impact via climate change. *Nat. Commun.* **7**, 12079 (2016).
40. C. J. Sprain *et al.*, The eruptive tempo of Deccan volcanism in relation to the Cretaceous–Paleogene boundary. *Science* **363**, 866–870 (2019).
41. P. M. Hull *et al.*, On impact and volcanism across the Cretaceous-Paleogene boundary. *Science* **367**, 266–272 (2020).
42. J. Surma, S. Assonov, D. Herwartz, C. Voigt, M. Staubwasser, The evolution of ^{17}O-excess in surface water of the arid environment during recharge and evaporation. *Sci. Rep.* **8**, 1–10 (2018).
43. K. A. Nagy, I. A. Girard, T. K. Brown, Energetics of free-ranging mammals, reptiles, and birds. *Annu. Rev. Nutr.* **19**, 247–277 (1999).
44. C. R. McKinney, J. M. McCrea, S. Epstein, H. A. Allen, H. C. Urey, Improvements in mass spectrometers for the measurement of small differences in isotope abundance ratios. *Rev. Sci. Instrum.* **21**, 724–730 (1950).
45. J. R. Hulston, H. G. Thode, Variations in the S33, S34, and S36 contents of meteorites and their relation to chemical and nuclear effects. *J. Geophys. Res.* **70**, 3475–3484 (1965).
46. E. D. Young, A. Galy, H. Nagahara, Kinetic and equilibrium mass-dependent isotope fractionation laws in nature and their geochemical and cosmochemical significance. *Geochim. Cosmochim. Acta* **66**, 1095–1104 (2002).
47. A. Pack *et al.*, The oxygen isotope composition of San Carlos olivine on the VSMOW2-SLAP2 scale. *Rapid Commun. Mass Spectrom.* **30**, 1495–1504 (2016).
48. Z. D. Sharp *et al.*, A calibration of the triple oxygen isotope fractionation in the SiO_2-H_2O system and applications to natural samples. *Geochim. Cosmochim. Acta* **186**, 105–119 (2016).
49. J. A. G. Wostbrock, E. J. Cano, Z. D. Sharp, An internally consistent triple oxygen isotope calibration of standards for silicates, carbonates and air relative to VSMOW2 and SLAP2. *Chem. Geol.* **533**, 119432 (2020).